Size and composition for 1-5 nm Ø PtRu alloy nano-particles from CuKα X-ray patterns

Baranova, Elena A.; Le Page, Yvon; Ilin, Dimitri; Bock, Christina; MacDougall, Barry; Mercier, Patrick H. J.

Publisher's version / Version de l'éditeur:
https://doi.org/10.1016/j.jallcom.2008.03.101
Journal of Alloys and Compounds, 471, 1-2, pp. 387-394, 2008-05-20

Journal of Alloys and Compounds 471 (2009) 387–394

Contents lists available at ScienceDirect

Journal of Alloys and Compounds

journal homepage: www.elsevier.com/locate/jallcom

Size and composition for 1–5 nm Ø PtRu alloy nano-particles from Cu Kα X-ray patterns

Elena A. Baranova*, Yvon Le Page, Dimitri Ilin, Christina Bock, Barry MacDougall, Patrick H.J. Mercier

Institute for Chemical Process and Environmental Technology (ICPET), National Research Council of Canada, Montreal Road 1200, Ottawa, ON, K1A 0R6 Canada

ARTICLE INFO

Article history:
Received 27 September 2007
Received in revised form 25 March 2008
Accepted 25 March 2008
Available online 20 May 2008

Keywords:
PtRu clusters
Nanostructured materials
Alloy
X-ray diffraction
Crystal structure

ABSTRACT

X-ray diffraction (XRD) studies on PtRu clusters with a range of diameters are reported. It is shown that for clusters smaller than 5 nm, Scherrer's formula is not adequate for the simultaneous interpretation of the size and composition of the clusters from their diffraction patterns. The theoretically and computationally developed approach is based on Debye's exact formula for scattering by randomly oriented molecules applied here to atomic models for the clusters. The novel approach interprets plausibly the same XRD patterns that Scherrer's formula could not. Pt_{1-x}-Ru_x nano-particles are synthesized with a modified polyol method and their size and composition are found from the interpretation of Cu Kα diffraction patterns using Debye's formula. The obtained results are consistent with both the chemical information and with previously reported results from other methods of investigation. Experimental profiles are shown to be affected here by non-uniformity of particle sizes.

1. Introduction

In a research program about platinum-based bi-metallic particles aimed at fuel cell and other electrocatalytic-based devices, we deal here with bi-metallic Pt-Ru catalysts that are of major interest as anode catalysts for direct methanol and reformate fuel cells [1,2]. Significant efforts have been devoted to their theoretical understanding, as well as synthesis and characterization [2–10]. As no single investigation method provides the required detailed structural information on bi-metallic nano-particles, the combination of several analytical methods is needed. Those methods include X-ray absorption spectroscopy (XAS) [3,4], nuclear magnetic resonance (NMR) [5], infrared spectroscopy [6,7], X-ray photoelectron spectroscopy (XPS) [8] and X-ray diffraction (XRD) [9–11]. We wish here to develop further the application of XRD because of the apparent simplicity of its application.

Recently, a rapid and straightforward method for the synthesis of Pt and bi-metallic Pt-Ru nano-catalysts has been developed [12]. In previous studies, mono- and bi-metallic particles of different size (1–5 nm) were synthesized [12,13]. The synthesis method was also utilized to prepare Pt-Ru nano-particles of different nominal compositions (Pt_{1-x}-Ru_x) [14]. Prepared as highly dispersed colloids and stabilized by a simple organic compound, they are amenable to structural, spectroscopic and electrochemical analysis. The structure and surface properties of these catalysts have been studied by infrared spectroscopy of adsorbed CO [13], high-resolution transmission electron microscopy (HRTEM), and electrochemical measurements (CO electro-oxidation) [12,14]. We would like here to investigate further the same nano-particles and characterize as accurately as possible their diameters and composition, and compare with our previous results. However, the diameter of these alloy nano-particles is so small that the simultaneous characterization of their diameter and ruthenium content presents a fundamental challenge for Scherrer's approximate formula [15], which is the state-of-the-art for interpretation of such patterns. In order to avoid the basic limitations of Scherrer's formula, we had to undertake theoretical, computational and practical developments involving Debye's exact formula [16] for diffraction by finite objects made of spherically symmetrical atoms, as detailed below.

2. Theory for interpretation of XRD patterns from Pt-Ru nano-particles

2.1. Inadequacy of Scherrer formula for estimating the size of nano-particles

$Pt_{1-x}Ru_x$ alloys are known to obey Vegard's law [17–19] in the range $x = 0$–0.6 where the alloy is face-centered cubic (fcc). Follow-

* Corresponding author. Tel.: +1 613 991 5683; fax: +1 613 941 2529.
E-mail address: olena.baranova@nrc-cnrc.gc.ca (E.A. Baranova).

0925-8388/$ – see front matter. Crown Copyright © 2008 Published by Elsevier B.V. All rights reserved.
doi:10.1016/j.jallcom.2008.03.101

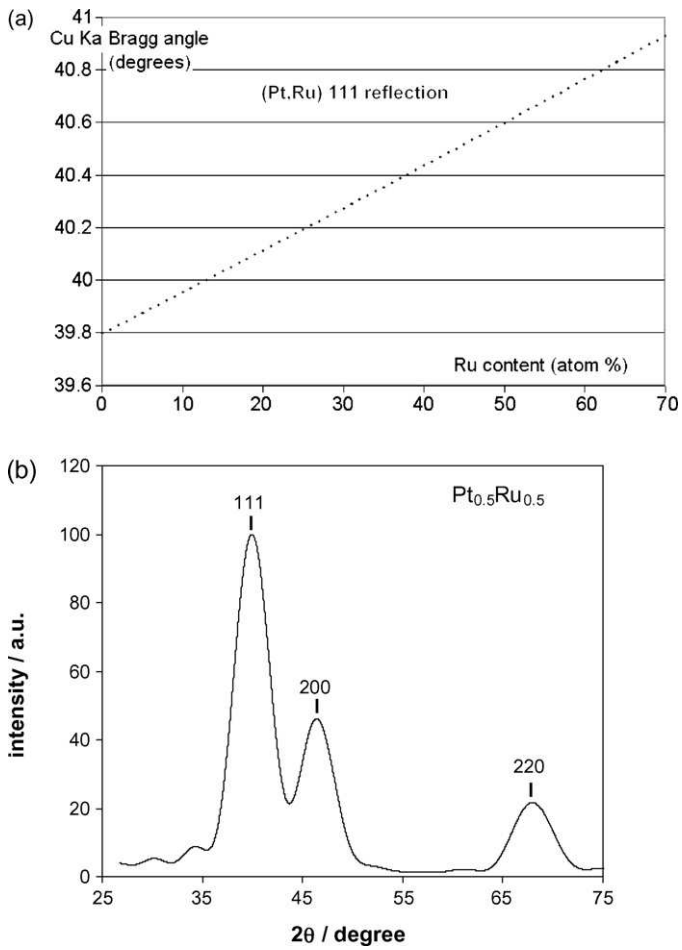

Fig. 1. (a) Cu Kα 2θ angle at maximum peak intensity for bulk (Pt, Ru) alloys *vs.* Ru composition for the alloy. (b) XRD pattern of Pt_{1-x}-Ru_x ($x = 0.5$) alloy nano-particles of 2.5 nm size.

ing [20], the linear fit for the cubic cell edge a is:

$$a(x) = 3.9231 - 0.1489x \quad (1)$$

Fig. 1a accordingly plots the 2θ Cu Kα Bragg angle for bulk $Pt_{1-x}Ru_x$ alloys as a function of the Ru atomic content x. Fig. 1b shows simulated X-ray powder patterns for crystalline powders of intermediate $Pt_{1-x}Ru_x$ alloy composition with $x = 0.5$, along with the $h\,k\,l$ indices of the diffraction peaks observed. Based on standard crystallographic calculations, both composition and particle size can then be extracted from scattering profiles for (Pt, Ru) crystalline powders. The Ru content x can be read off in Fig. 1a by reporting on it the peak's Cu Kα Bragg angle 2θ. The particle size can then be extracted from the full-width at half-maximum (FWHM) of any of the diffraction peaks through the well-known Scherrer formula [15]:

$$D = \frac{K\lambda}{\mathrm{FWHM}\,\cos\theta} \quad (2)$$

where λ is the wavelength and K is a numerical constant with value close to 0.88. Provided that FWHM is expressed in radians, the units of D are those of λ.

In the strategy outlined above, however, it is implicitly assumed that neighboring peaks 1 1 1 and 2 0 0 add up in intensity in the region where they overlap on the powder pattern. For Pt fcc material, this assumption is essentially justified for crystallite sizes greater than 5 nm (see Fig. 3 below and associated discussion). For crystallites with a smaller size, the spread of measured intensities around reciprocal nodes becomes so large that neighboring reflections 1 1 1 and 2 0 0 start overlapping, not just on the powder pattern, but also in reciprocal space. The contributions of the overlapping nodes add up in amplitude rather than intensity at each point of reciprocal space. As shown in Section 4.1 below, this displaces the Bragg angle from the value expected from the intensity overlap.

2.2. Modeling with Debye's formula for scattering by randomly oriented molecules

Debye [16] established the following simple but exact formula for the scattering by randomly oriented molecules made of spherically symmetrical atoms:

$$|F(R)|^2 = \sum_{m=1,N}\sum_{n=1,N} f_m(R) f_n(R) \frac{\sin(2\pi R\, d_{mn})}{2\pi R\, d_{mn}} \quad (3)$$

where $F(R)$ is the scattering amplitude in electrons at reciprocal length R, N is the number of atoms in the molecule, $f_m(R)$ is the scattering factor in electrons of atom m at reciprocal length R in $Å^{-1}$ while d_{mn} is the distance in Å separating atoms m and n in the molecule. This formula can then be used to compute exact scattering profiles for models of nano-particles treated like molecules.

2.3. Implementation of Debye's formula

Pt nano-crystals with <5 nm diameter contain less than 5000 atoms, and their X-ray scattering profiles are accordingly easily amenable to calculations with present-day PCs. *Materials Toolkit* [21] includes a tool to create files with Cartesian coordinates for atoms constituting spherical or cylindrical clusters. It includes another tool to compute the scattering pattern of finite objects with Debye's formula (3) above, making the following application relatively straightforward. The nine-coefficient scattering factor curves for f_m and f_n were those from data in [22].

We have accordingly created a number of spherical Pt nano-crystals centered either at a Pt atom, a tetrahedral site or an octahedral site of the Cu fcc structure type. This was performed by accepting only atoms whose centre is within a given radius from the selected centre. We then calculated the scattering profile for the cluster using Debye's formula.

Two different routes can be taken for analysis of computation of results, in view of comparison with experimental results. We could reduce the experimental intensity data into values of $|F|^2$ and reciprocal lengths R through application of Lorentz-polarization (LP) corrections and thermal-motion corrections, followed by use of reciprocal lengths instead of Bragg angles. Comparison with numbers coming out of Debye's formula would then be direct, but readers would have to manipulate their data intensively before being able to make use of the information reported here. We instead chose to perform the opposite, namely back-correction of Debye's $|F|^2$ values for the LP factor assuming unpolarized Cu Kα radiation and Bragg–Brentano diffraction geometry. We also used Bragg angles instead of R-values. Experimentalists can then directly compare uncorrected Cu Kα raw measured data with results reported here. The only correction left to experimentalists would then be an optional isotropic thermal-motion correction whose magnitude cannot be anticipated here. We of course selected the second route because it facilitates the application of results reported below.

3. Experimental

3.1. Synthesis of the nano-particles

Synthesis of Pt and Pt-Ru nano-particles was carried out in ethylene glycol (EG) (Anachemia, ACS grade) solutions. The particle size is varied via the synthesis solu-

Table 1
Synthesis conditions of Pt and Pt-Ru nano-particles prepared using the co-reduction of precursor salts method

Nano-particle	m_{PtCl_4} (g)	m_{RuCl} (g)	V_{EG} (mL)	C_{NaOH} (M)
Pt	0.4652	–	50	0.1–0.2
$Pt_{0.5}$-$Ru_{0.5}$	0.2326	0.1383	50	0.08–0.11
$Pt_{0.67}$-$Ru_{0.33}$	0.2326	0.0692	50	0.07
$Pt_{0.75}$-$Ru_{0.25}$	0.2326	0.0346	50	0.065
$Pt_{0.86}$-$Ru_{0.14}$	0.2326	0.0231	50	0.055

tion pH that is adjusted using different concentrations of sodium hydroxide (EM Science) as described in previous work [12]. Two synthesis methods were employed, namely (i) co-reduction of mixed precursor salts and (ii) step reduction of the precursor salts.

3.1.1. Co-reduction of mixed precursor salts

Details of the synthesis of the colloidal Pt and Pt-Ru solutions of different size using the co-reduction method are described in previous works [12,13]. In short, metal salts of $PtCl_4$ and $RuCl_3$ (Alfa Aesar, 99.9% metals basis) were dissolved in 50 mL of ethylene glycol containing NaOH. The solutions were stirred for 30 min., subsequently heated and refluxed for 3 h at 160 °C. Dark brown solutions containing either Pt or Pt-Ru colloids were formed rapidly (<15 min.) in this manner. Table 1 shows the synthesis conditions for mono-metallic Pt nano-particles and Pt-Ru bi-metallic particles prepared by the co-reduction of mixed precursor salts.

3.1.2. Step reduction of precursor salts

3.1.2.1. Bi-metallic Pt/Ru particles prepared from preformed Pt colloids. Pt to Ru ratios of 0.67:0.33—Step 1: 0.2326 g of $PtCl_4$ (Alfa Aesar, 99.9% metal basis) were dissolved in 25 mL of ethylene glycol containing 0.07 M NaOH. The solution was stirred for 30 min at room temperature, and subsequently heated under reflux at 160 °C for 1 h. A dark brown solution containing Pt colloids was formed in this manner. The initial pH of the synthesis solution was 11, while after reflux it dropped to 7.

Step 2: 0.0692 g $RuCl_3$ (Alfa Aesar, 99.9% metal basis) was dissolved in 25 mL of ethylene glycol containing 0.02 M NaOH, followed by stirring for 30 min at room temperature. The pH of the solution was 7 after complete dissolution of the precursor salts.

Step 3: The "in step 2" prepared solution of the Ru-precursor salt was added to the colloidal Pt solution prepared in step 1. The mixture was stirred for 30 min at room temperature, followed by heating under reflux at 160 °C for 3 h. Dark brown solutions of a pH of 6 containing Pt/Ru colloids were formed. The resulting solutions containing Pt-Ru colloids are referred to as $Pt_{0.67}/Ru_{0.33}$ nano-particles prepared by the "step synthesis method with preformed Pt colloids".

Pt to Ru ratios of 0.33:0.67—The same procedure was employed but the initial amount of $PtCl_4$ was 0.1166 g and the concentration of NaOH was 0.06 M, while the amount of $RuCl_3$ was taken as 0.1383 g. The pH of the final solution was 7.

3.1.2.2. Bi-metallic Ru/Pt nano-particles prepared from preformed Ru colloids. Pt to Ru ratios of 0.5:0.5—Step 1: 0.1383 g of $RuCl_3$ (Alfa Aesar, 99.9% metal basis) were dissolved in 25 mL of ethylene glycol (Anachemia, ACS grade) containing 0.1 M NaOH. The solution was stirred for 30 min at room temperature, and then heated under reflux at 160 °C for 1 h. A dark brown solution containing Ru colloids was formed in this manner. The initial pH of the synthesis solution was 9.5, while after reflux it dropped to 7.

Step 2: 0.2326 g $PtCl_4$ (Alfa Aesar, 99.9% metal basis) was dissolved in 25 mL of ethylene glycol containing 0.06 M NaOH and stirred for 30 min at room temperature. The pH of the solution was 7 after complete dissolution of the precursor salt.

Step 3: The "in step 2" prepared solution of the Pt-precursor salt was added to the colloidal Ru solution prepared in step 1. The mixture was stirred for 30 min at room temperature, followed by heating under reflux at 160 °C for 3 h. Dark brown solutions of pH 5.5 containing Ru/Pt colloids were formed.

Pt to Ru ratios of 0.67:0.33—The same procedure as for the ratio 0.5:0.5 was employed but the initial amount of Ru was 0.0692 g and the NaOH concentration was 0.05 M. The resulting solutions are referred to as Ru/Pt nano-particles prepared by the "step synthesis method with preformed Ru colloids".

3.2. Numerical calculation of scattering profiles for Pt nano-particles

Calculations of scattering profiles for Pt clusters containing between 100 and 600 atoms were performed with *Materials Toolkit* [21]. Those calculations were carried out as detailed in Section 2 above, with the nano-particle considered to be a molecular object. Fig. 2 shows the results of pattern simulations calculated for Pt nano-particle models with diameters comprised between 1 and 5.0 nm. The line width of the two dominant peaks, corresponding to reflections Pt(1 1 1) and Pt(2 0 0) with crystalline powders, increases continuously with smaller particle size before merging into a single broad peak for Pt nano-crystals with diameter below 1.6 nm.

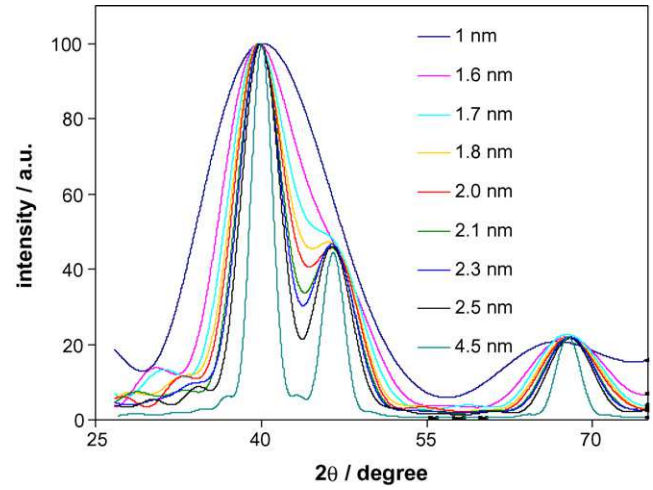

Fig. 2. Simulated XRD patterns of Pt nano-particles with various diameters as indicated.

For ease of comparison between theory and experiment, we did not use the origin of intensities as the zero height for the peak because that would have been quite difficult to ascertain experimentally. We rather used the minimum intensity (number of counts) between reflections 2 0 0 and 2 2 0 around 55°2θ for this purpose. Half-height and 3/4 height for the peak are accordingly defined by the maximum peak intensity and minimum intensity defined in that way.

Comparison with experiment requires accurate location of intensity maximum for a diffraction peak that is both not very intense and spans several degrees at 3/4 maximum. Tests with fitting third-degree polynomials over the peak top of profiles calculated with Debye's formula showed that the maximum of the fitted curve corresponded quite accurately with the 2θ angle for maximum intensity calculated with Debye's formula. This fit was usually within a hundredth of a degree for a wide variety of cluster diameters. This observation was verified irrespective of the exact cutoff height of data points for the fit that we took over the top 80–90% of maximum peak height. As the expression for the fitted cubic polynomial is very much conditioned by the precise shape of the intensity decrease on both sides of the peak top, we therefore collected experimental intensities with extra care over that peak top by using very long counts and small angular steps.

3.3. X-ray diffraction measurements

A Scintag XDS2000 system was employed using a Cu Kα source to obtain experimental XRD patterns of the dried colloids. The Bragg angle extended from 2θ of 25 to 70°2θ and was varied using a step size of 0.06°2θ, accumulating data for 60 s per step. Samples were prepared by placing 50 μL of the colloidal solution on a low-background single-crystal Si (510) plate (Gem Dugout), followed by drying in air at 80 °C for 1 h. The maximum-intensity peak position ($2\theta_{max}$) for the overlapping 1 1 1/2 0 0 peak was extracted from a cubic fit to the top 10–20% of the experimental intensities around 40°2θ Cu Kα Bragg angle. The full-width at 3/4 (FW3/4M) and at half (FWHM) of the maximum height of that peak were determined assuming the minimum intensity measured around 55°2θ as the zero height, while the peak height was the maximum intensity measured around 40°2θ. Table 2 summarizes the values of $2\theta_{max}$, FW3/4M and FWHM extracted from the experimental XRD patterns measured for all synthesis products that were analyzed.

4. Results and discussion

We implement here Debye's formula (Eq. (3)) for two purposes: (i) to interpret the diffraction patterns from pure Pt and alloy $Pt_{1-x}Ru_x$ nano-particles with fcc structure; and (ii) to extend this information into establishing a methodology for estimating the size and composition of fcc Pt_{1-x}-Ru_x nano-particles using only X-ray powder diffraction.

In agreement with previous experiments [18] and *ab initio* work [20], we assume the $Pt_{1-x}Ru_x$ alloy system to obey Vegard's law from bulk to nano-particulate material. For bulk material, it was not possible to distinguish visually a curvature away from the linear relationship predicted by Vegard's law in the cubic cell edge *a* versus composition graph (see Fig. 2a in Ref. [20]). From numerical analysis of the energy versus composition graph (Fig.

Table 2
Summary of slow scan XRD results on Pt and Pt-Ru nano-particles

Nano-particle	Synthesis method	pH	Particle size (nm)	$2\theta_{max}$ (°)	FWHM (°)	FW3/4M (°)	Composition of PtRu alloy (error 5–10%)
Pt	Reduction in EG	7	1.5 ± 0.1	39.50	7.9	4.5	
Pt		6	2.4 ± 0.1	39.57	3.9	2.2	n.a.
Pt		5	3.3 ± 0.6	39.68	3.1	1.8	
Pt		4.5	4.3 ± 0.3	39.76	2.7	1.3	$Pt_{87}Ru_{13}$
$Pt_{0.5}$-$Ru_{0.5}$	Co-reduction in EG	7	1.4 ± 0.4	39.61	7.5	4.6	$Pt_{58}Ru_{42}$
$Pt_{0.5}$-$Ru_{0.5}$		6	2.1 ± 0.2	40.22	5.2	2.8	
$Pt_{0.5}$-$Ru_{0.5}$		5.5	2.4 ± 0.3	39.93	4.8	2.2	$Pt_{56}Ru_{44}$
$Pt_{0.67}$-$Ru_{0.33}$	Co-reduction in EG	6	1.8 ± 0.2	39.84	7.2	3.8	$Pt_{71}Ru_{29}$
$Pt_{0.75}$-$Ru_{0.25}$		6	2.0 ± 0.3	39.82	5.3	2.9	$Pt_{82}Ru_{18}$
$Pt_{0.86}$-$Ru_{0.14}$		6	2.1 ± 0.3	39.93	5.0	3.2	$Pt_{77}Ru_{23}$
$Pt_{0.67}/Ru_{0.33}$	Step reduction Pt + $RuCl_3$ in EG	6	1.9 ± 0.1	39.65	5.5	2.9	$Pt_{85}Ru_{15}$
$Pt_{0.33}/Ru_{0.67}$		7	1.7 ± 0.1	40.06	6.4	4.1	$Pt_{55}Ru_{45}$
$Ru_{0.5}/Pt_{0.5}$	Step reduction Ru + $PtCl_4$ in EG	5.5	1.9 ± 0.2	40.94	6.9	3.5	n.a.
$Ru_{0.33}/Pt_{0.67}$		6	1.7 ± 0.1	40.28	6.7	4.0	n.a.

2b in Ref. [20]), it was also shown [20] that the energy difference $\varepsilon = U_{PtRu} - (U_{PtPt} + U_{RuRu})/2$ for bonds involving, respectively, Pt–Ru, Pt–Pt and Ru–Ru bonds is much lower than the thermal activation energy kT at even room temperature. As this energy difference ε is at the root of non-random pair distribution in binary solid-solution alloys, it can then be concluded that $Pt_{1-x}Ru_x$ alloys both obey Vegard's law and display random atom type distributions as closely as could be determined.

4.1. Shift of peak position and broadening with decreasing particle size

Figs. 3–5 report 2θ Cu Kα at maximum intensity, FWHM and full-width at 3/4 maximum values for the Pt 1 1 1/2 0 0 peak *vs.* the cluster size. The values are all extracted numerically from the results of the above simulations (Section 3.2) implementing Debye's formula on a series of spherical cluster models with three distinct choices of position for their centre (Section 2.3). These figures will be used below to extract the average particle size (Figs. 4 and 5) and to correct the 2θ maximum position for the diffraction effects related to the nano-particles.

In Appendix A, we show that diffraction by a collection of nano-particles of a perfect solid-solution alloy is basically that of the average nano-particle sitting on a fairly uniform intensity background. That background gets discarded in the numerical analysis presented here. With Vegard's law, like here, the average nano-particle is made of atoms with average atom radius and average electron density. If the Fourier transform of $f(\mathbf{x})$ is $F(\boldsymbol{X})$, the well-known scaling property of Fourier transforms states that the Fourier transform of $f(k\mathbf{x})$ is $F(\boldsymbol{X}/k)/k$. It follows that a small contraction in the cubic parameter a of the alloy causes a slight commensurate expansion of its diffraction pattern with no other change. As the change of parameter a from pure Pt to 50/50 PtRu alloys would be a contraction by at most 1.9%, the effect on Figs. 3–5 is therefore a corresponding rescaling by the same value for reciprocal values and therefore diffraction angles. This is within the spread of the data for

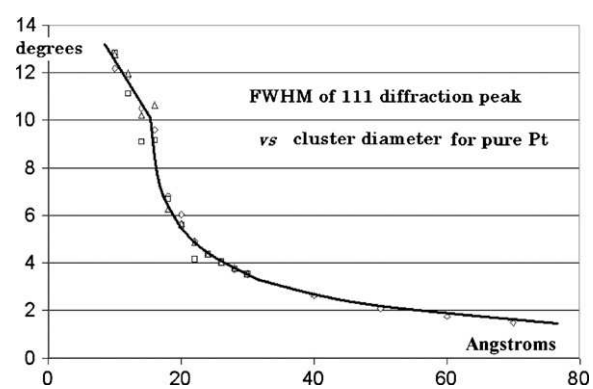

Fig. 4. Cu Kα full-width at half-maximum for Pt clusters *vs.* cluster diameter in Angstroms. Symbols for cluster center: at Pt, diamonds; at tetrahedral site, triangles; at octahedral site, squares.

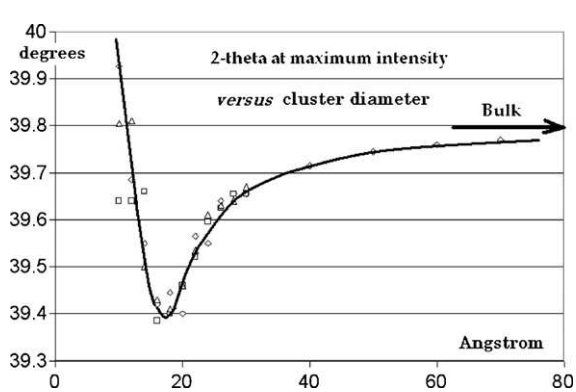

Fig. 3. Cu Kα 2θ angle at maximum peak intensity for Pt clusters *vs.* cluster diameter in Angstroms. Symbols for cluster center: at Pt, diamonds; at tetrahedral site, triangles; at octahedral site, squares.

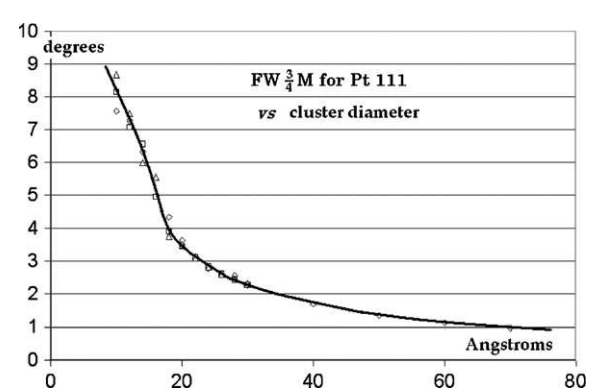

Fig. 5. Cu Kα full-width at 3/4 maximum for Pt clusters *vs.* cluster diameter in Angstroms. Symbols for cluster center: at Pt, diamonds; at tetrahedral site, triangles; at octahedral site, squares.

the various origins of nano-particles. Figs. 3–5 can then be used as printed, whatever the composition of the (Pt, Ru) alloy.

4.2. Size distribution of Pt nano-particles

Experimental XRD patterns for the four Pt colloids are presented in Fig. 6. The peaks around 40, 46 and 68°2θ correspond to Pt reflections 1 1 1, 2 0 0 and 2 2 0, respectively. The sharp peaks at 2θ values of 27.34, 31.69, 45.45, 56.48 and 66.23°2θ, represent the reflections of crystalline NaCl present as a result of the synthesis procedure [12].

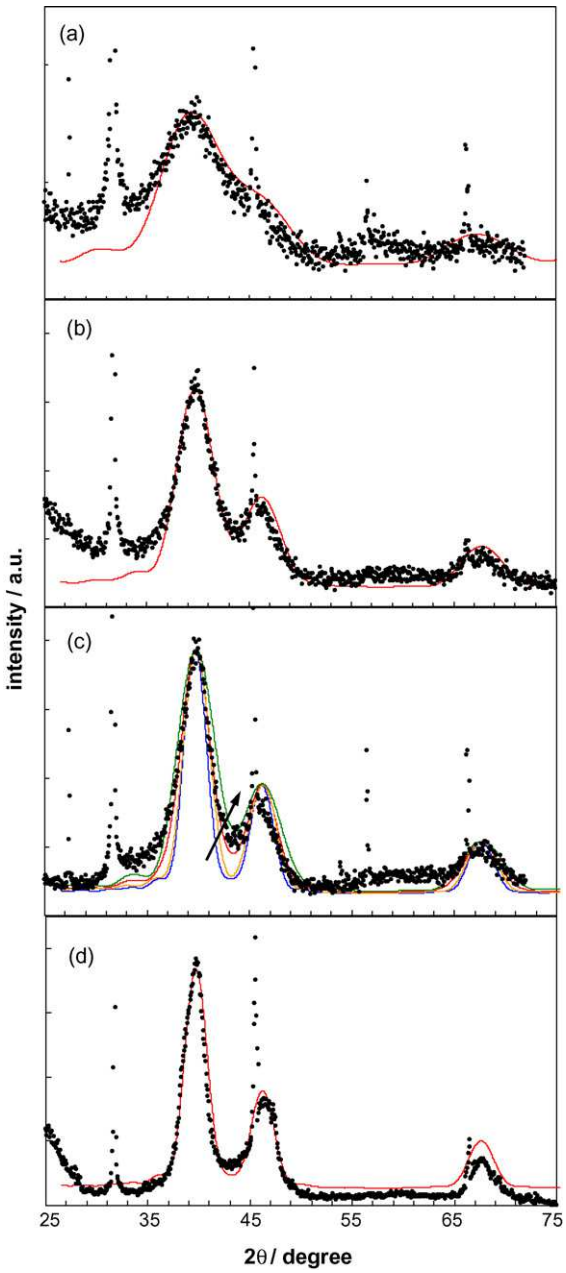

Fig. 6. Slow scan experimental (symbols) and simulated (solid line) XRD patterns for Pt colloids of different size. (a) 1.5 nm, simulated spectrum consists of 50% of 1.4 nm and 50% of 1.6 nm; (b) 2.4 nm, simulated pattern consists of 50% of 2.3 nm and 50% of 2.5 nm particles; (c) 3.3 nm, Simulated patterns for particles of the uniform particle size and weighted average of the uniform particle size models (50% 2.7 nm, 25% of 3.5 nm and 25% of 4.0 nm). As indicated by arrow from bottom to top: model of 4.0 nm; model of 3.5 nm; model of 50% 2.7 nm, 25% of 3.5 nm and 25% of 4.0 nm; model of 2.7 nm particles. (d) 4.3 nm, simulated pattern consists of 50% 4 nm and 50% of 4.5 nm.

Precise Bragg angles for the Pt colloids (Table 2) were derived from a third-order polynomial fit to the profile counts close to the top of the peak as described in Section 3.2. These values are in good agreement with those extracted numerically from the 2θ Cu Kα results of the simulations implementing Debye's formula (Fig. 3), and differ significantly from the 39.7645°2θ value expected for bulk Pt [23]. This shows supporting evidence that the Debye formula is adequate for interpreting the shift in position of Bragg angles arising from the nano-size dimension of the synthesized Pt particles.

However, the widths of diffraction lines observed on the experimental patterns are greater than those obtained from simulations of clusters with uniform particle size (Fig. 2). This is demonstrated in Fig. 6, which shows simulated XRD patterns (solid lines) obtained by taking into account the size non-uniformity of the resulting Pt nano-particles. This was done by performing a weighted average of several patterns of models corresponding to different uniform particle size (indicated in the figure caption), as illustrated in Fig. 6c, which shows simulations corresponding to 50% of 2.7 nm clusters, 25% of 3.5 nm and 25% of 4.0 nm clusters along with the models for uniform particle size. The width of the observed diffraction lines could not have been accounted for using simulations corresponding to uniform particle size clusters.

4.3. Size and composition of Pt-Ru nano-particles prepared by co-reduction synthesis

Figs. 7 and 8 show experimental XRD patterns for the Pt-Ru colloids prepared using the co-reduction method. Two distinct diffraction peaks around 40 and 46°2θ are observed, indicating the formation of a Pt fcc lattice for these Pt-Ru nano-particles. Again, the sharp peaks at 2θ maximum of 27.34, 31.69, 45.45, 56.48 and 66.23°2θ are due to crystalline NaCl. As in the case of mono-metallic Pt particles, the size analysis of the Pt-Ru nano-particles from the XRD data is based on full-width at half height (FWHM) and full-width at 3/4 height of the Pt(1 1 1) peak according to Figs. 4 and 5.

Fig. 7 shows XRD of $Pt_{0.5}$-$Ru_{0.5}$ colloids of three different size 1.4, 2.1, 2.4 nm and corresponding interference powder-pattern simulations with spherical Pt nano-crystals centered at a Pt atom. As seen from the figure, the relation between experiment and theory is satisfactory. The structure is face centered cubic (fcc) for all three $Pt_{0.5}$-$Ru_{0.5}$ colloids prepared by co-reduction of Pt and Ru precursor salts. Fitting third-degree polynomials over the (1 1 1) peak top of XRD profiles for the $Pt_{0.5}$-$Ru_{0.5}$ colloids shows the following 2θ maximum position (2θ_{exp}): 39.93, 40.22, 39.61°2θ for 2.4, 2.1 and 1.4 nm particles, respectively. To extract the exact particle composition, first we need to correct particle size for the predicted diffraction effect. Knowing particle size from the average of the two diameters (FWHM and FW3/4M) and using Fig. 3, we can find Cu Kα angles corresponding to the pure Pt particles of the same size. The difference between experimentally found 2θ_{exp} values for Pt-Ru particles and theoretical 2θ_{th} for Pt clusters from Fig. 3 will give a correction factor (C). Therefore, the true angle (T) for a bulk sample with the same composition as the Pt-Ru nano-particles is $T = 39.7645° + C$, where 39.7645° is 2θ maximum of fcc (1 1 1) for bulk Pt [23]; C is a correction factor.

Using the found T value for the Cu Kα angles, we can read the composition of the corresponding equivalent bulk sample off Fig. 1. The calculations suggest that PtRu alloys of the following Pt:Ru at.% ratios are formed: 56:44 for 2.4 nm; 58:42 for 2.1 nm and 87:13 for 1.4 nm Pt-Ru particles, as also listed in Table 1. An error of ±5–10 at.% is estimated for these calculations.

Furthermore, Ru appears to be fully dissolved in the Pt fcc lattice, as the nominal Pt:Ru ratio is similar to the suggested Pt:Ru alloy ratio. However, for the smaller 1.4 nm particles, the Ru is not completely dissolved in the Pt fcc lattice, as suggested by the 87:13 at.%

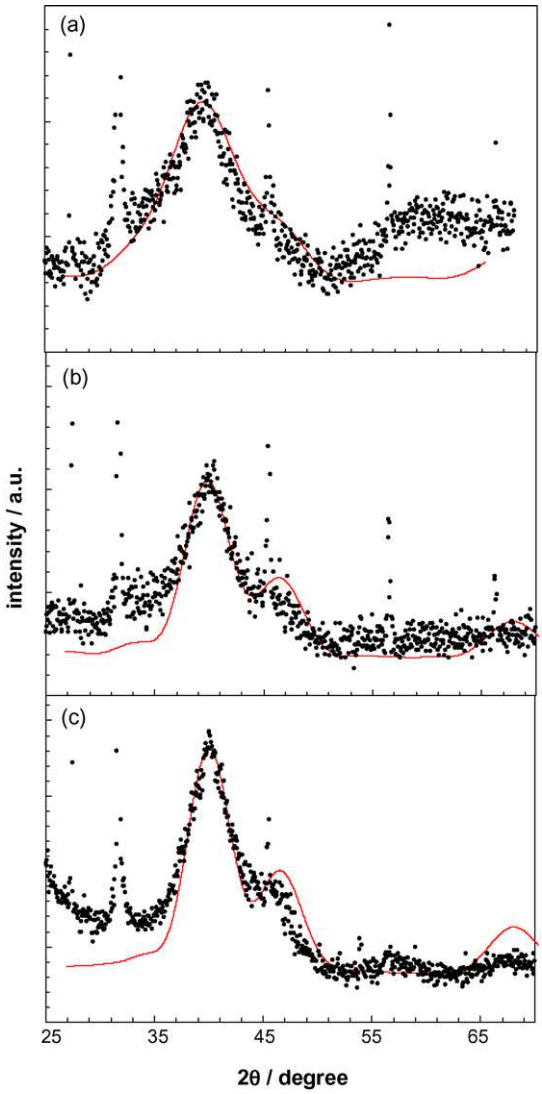

Fig. 7. Slow scan experimental (symbols) and simulated (solid line) XRD patterns for Pt-Ru particles of different size prepared by the co-reduction method. Nominal composition is $Pt_{0.5}$-$Ru_{0.5}$. (a) 1.4 nm particle size. Simulated pattern consists of 33% of 1.0 nm, 33% of 1.5 nm and 33% of 1.8 nm; (b) 2.1 nm. Simulated pattern consists of 50% of 2.0 nm and 50% of 2.3 nm; (c) 2.4 nm. Simulated pattern consists of 33% 2.7 nm, 33% of 2.3 nm and 33% of 2.0 nm.

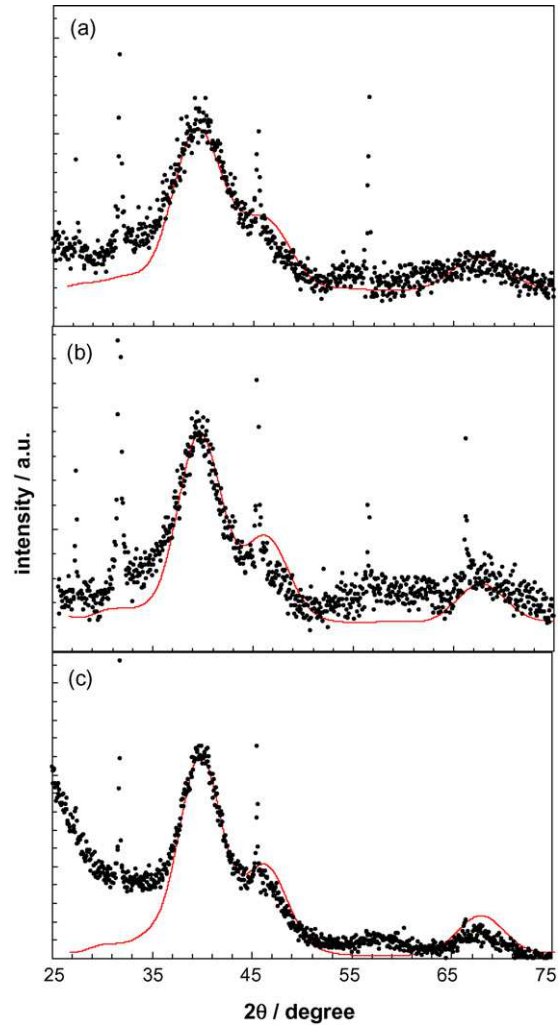

Fig. 8. Slow scan experimental (symbols) and simulated (solid line) XRD patterns for Pt-Ru particles prepared by the co-reduction method with different nominal Pt:Ru at. composition: (a) $Pt_{0.67}$-$Ru_{0.33}$, particle size is 1.9 nm. Simulated pattern consists of 33% of 2.1 nm, 33% of 1.8 nm and 33% of 1.7 nm; (b) $Pt_{0.75}$-$Ru_{0.25}$, particle size is 2.0 nm. Simulated pattern consists of 50% of 2.3 nm and 50% of 1.7 nm; (c) $Pt_{0.86}$-$Ru_{0.14}$, particle size is 2.1 nm. Simulated pattern consists of 70% 2.3 nm and 30% of 1.6 nm.

Pt:Ru alloy ratio. Based on previous results [24], it is believed that smaller particles are not alloyed, as alloy formation for particles of less than 1 nm diameter is believed to be impossible due to the fact that Pt self-surface segregates (even at low temperatures) and that for smaller particles the majority of the atoms are surface atoms.

Fig. 8 shows experimental and simulated XRD patterns, obtained for the Pt-Ru nano-particles of different compositions ($Pt_{0.67}$-$Ru_{0.33}$, $Pt_{0.75}$-$Ru_{0.25}$, $Pt_{0.86}$-$Ru_{0.14}$), but similar particle size (2.0 ± 0.1 nm). Table 2 shows the values for the average particle size of the three particles calculated using full-width at half height (FWHM) and full-width at 3/4 height (FW3/4M) of the Pt(1 1 1) peak (Figs. 4 and 5). The position of the Pt(1 1 1) peak for all three catalysts is shifted to higher 2θ positions (39.84, 39.82 and 39.93°2θ for $Pt_{0.67}$-$Ru_{0.33}$, $Pt_{0.75}$-$Ru_{0.25}$, $Pt_{0.86}$-$Ru_{0.14}$) than for the mono-metallic Pt nano-particles of the same size (Fig. 3). Using the above described procedure for the extraction of particle composition, we found that PtRu alloys of the following Pt:Ru at.% ratio are formed: 71:29 for $Pt_{0.67}$-$Ru_{0.33}$, 82:18 for $Pt_{0.75}$-$Ru_{0.25}$, 77:23 for $Pt_{0.86}$-$Ru_{0.14}$, as also listed in Table 2. Within the estimated ±5–10 at.% error of these calculations, the experimental data are in agreement with the nominal synthesis compositions.

4.4. Pt/Ru particles prepared by step reduction starting from preformed Pt colloids

Successive synthesis of Pt/Ru nano-particles starting from preformed Pt colloids was carried out in the present work. Two kinds of bi-metallic particles with different overall Pt to Ru ratios (0.67:0.33 and 0.33:0.67) were synthesized first, by forming Pt clusters and subsequently reacting with a Ru-salt solution. Successive reduction of two metal salts is considered as one of the most suitable methods to prepare core-shell structured bi-metallic nano-particles [25–27]. In a core-shell structure, one metal element forms an inner core whereas the other element surrounds the core to form a shell. Examples of core-shell structures have been observed in PVP-stabilized (poly(*N*-vinyl-2-perrolidon)) Pd-Pt bi-metallic nano-particles, Au-Pd and Au-Pt [26–29].

Experimental and theoretical XRD patterns of $Pt_{0.67}/Ru_{0.33}$ and $Pt_{0.33}/Ru_{0.67}$ colloids are shown in Fig. 9. The good agreement

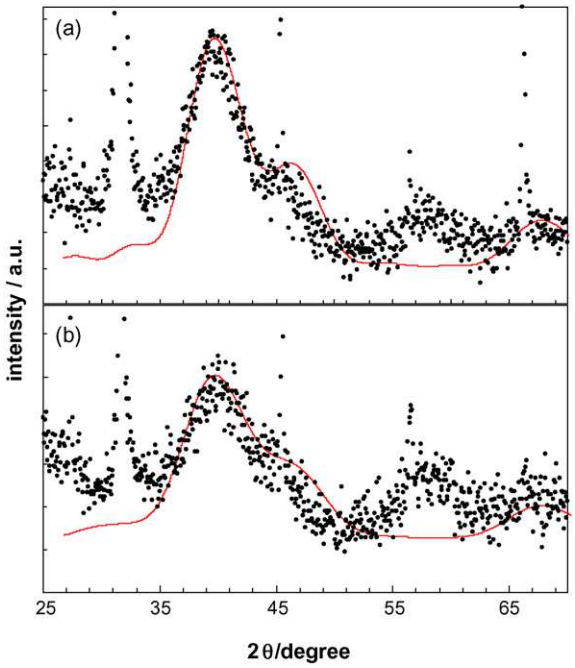

Fig. 9. Slow scan experimental (symbols) and simulated (solid line) XRD patterns for Pt-Ru particles of different composition prepared by the step synthesis, starting from preformed Pt colloids. Note: The peak at around 60°2θ is spurious and originates in the "zero background" silicon support. (a) $Pt_{0.67}/Ru_{0.33}$, particle size is 1.9 nm. Simulated pattern consists of 50% 1.8 nm and 50% of 2.0 nm; (b) $Pt_{0.33}/Ru_{0.67}$, particle size is 1.7 nm. Simulated pattern consists of 50% 1.6 nm and 50% of 1.8 nm.

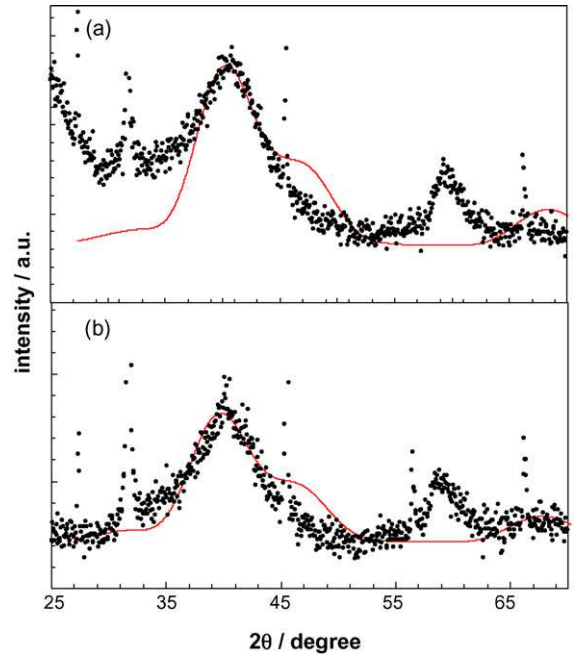

Fig. 10. Slow scan experimental (symbols) and simulated (solid line) XRD patterns for Ru-Pt particles of different composition prepared by the step synthesis method, starting from preformed Ru colloids. Note: The peak at around 60°2θ is spurious and originates in the "zero background" silicon support. (a) $Ru_{0.5}/Pt_{0.5}$, particle size is 1.9 nm. Simulated pattern consists of 25% of 1.6 nm, 25% of 1.7 nm, 25% of 1.9 nm and 25% of 2.0 nm; (b) $Ru_{0.33}/Pt_{0.67}$, particle size is 1.7 nm. Simulated pattern consists of 33% of 1.6 nm, 33% of 1.7 nm and 33% of 1.8 nm.

between theory and experiment indicates that the final particles are fcc alloys similar to the co-reduced Pt-Ru colloids. The 2θ position of the Pt(1 1 1) peak for the Pt/Ru colloids is shifted to higher values (39.65 and 40.06°2θ for $Pt_{0.67}/Ru_{0.33}$ and $Pt_{0.33}/Ru_{0.67}$, respectively), compared to the pure Pt fcc clusters of the same size suggesting formation of a PtRu alloys. Estimated composition of the Pt:Ru solid solutions in at.% is 85:15 for $Pt_{67}/Ru_{0.33}$ and 55:45 for $Pt_{0.33}/Ru_{67}$, as also listed in Table 2. The analyzed alloy composition indicates that Pt-Ru bi-metallic particles are formed during the step synthesis starting from preformed Pt colloids and not just a mixture of single Pt and Ru phases. However, the alloy compositions differ from the nominal 67:33 and 33:67 at. %, and this may indicate that some amount of Ru is present as a mono-metallic phase.

The plausible interaction mechanism of preformed Pt colloids with Ru^{III} ions is seed-mediated deposition. According to this mechanism, the Pt colloids formed in the first step serve as seeds for Ru^{III} ions adsorption and deposition leading to formation of Pt/Ru bi-metallic particles. Due to the step deposition, the resulting particles may adopt a Pt-core-Ru-shell structure [27]. Indeed, the enrichment of nano-particle surface by Ru atoms was observed using IR measurements of adsorbed CO molecules (not presented here). The activity of the Pt/Ru particles towards CO_{ads} electro-oxidation is high and comparable to the alloyed Pt-Ru particles of the same size and composition prepared by the co-reduction method. According to these arguments, and the fact that Pt tends to surface segregate, it is believed that the resulting particles are fcc alloys rather than true core-shell structures.

4.5. Ru-Pt particles prepared by step reduction starting from preformed Ru colloids

Fig. 10 shows slow scan X-ray diffraction patterns and corresponding theoretical patterns for $Ru_{0.5}/Pt_{0.5}$ and $Ru_{0.33}/Pt_{0.67}$ nano-particles prepared by the step reduction of the precursor salts (first, by forming Ru nano-particles that are subsequently reacted with a Pt-salt solution). It was recently demonstrated that formation of Ru/Pt particles occurs due to the difference in redox potential of Pt and Ru [14]. When Pt ions are added in the presence of Ru nano-particles, some Ru^0 atoms on the nano-particles are oxidized and reduce Pt^{II} ions to Pt^0 atoms. After the reduction of Pt^{II} ions, the oxidized Ru ions are reduced by ethylene glycol and redeposited forming Ru/Pt nano-particles. As seen from Fig. 10, the experimental XRD patterns contain only one dominant peak at 40.94 and 40.28°2θ for $Ru_{0.5}/Pt_{0.5}$ and $Ru_{0.33}/Pt_{67}$, respectively. This feature is characteristic for PtRu clusters with diameters below 1.6 nm for which the spread of reciprocal nodes becomes so large that reflections 1 1 1 and 2 0 0 are overlapping and a single broad peak is observed. However, the absence of the Pt (2 0 0) diffraction peak cannot be explained in this way since the diameters of the resulting particles are larger than 1.5 nm. The average particle sizes estimated from the XRD data for these particles are 1.9 and 1.8 nm for the $Ru_{0.5}/Pt_{0.5}$ and $Ru_{0.33}/Pt_{0.67}$ colloids, respectively. These average particle sizes are in good agreement with the particle sizes obtained from the TEM images taking differences between the two methods into account [14]. The shift in the 2θ maxima position reveals the formation of bi-metallic Ru/Pt particles and not single Pt and Ru phases, while the absence of the 2 0 0 reflection may indicate that the resulting particles are not fcc solid solutions and their analysis by the method described above is not appropriate. At the same time, they do not display the hexagonal close-packed structure expected for a mono-metallic Ru phase with the dominant peak for the Ru (1 0 1) plane at 44°2θ.

Based on the data presented above, it is concluded that the step reduction method starting from preformed Pt colloids results in fcc PtRu alloys. The amount of Ru dissolved in the fcc Pt differs from the nominal composition suggesting that some of the Ru is also present as a single Ru phase. In case of the Ru/Pt particles made by

the step reduction method starting from preformed Ru colloids, the XRD results suggest that fcc PtRu alloys are not present.

5. Conclusion

Through synthesis of pure-platinum nano-particles with a range of diameters, we have demonstrated experimentally the inadequacy of Scherrer's formula for the simultaneous interpretation of their diameters and composition from their diffraction patterns. We have accordingly developed theoretically and computationally a novel approach based on Debye's exact formula. We have shown that this new approach could be used to interpret the same patterns that Scherrer's formula could not. We prepared a range of Pt_{1-x}-Ru_x nano-particles by the modified polyol method. From interpretation of Cu Kα diffraction patterns in the way developed above, we reach conclusions about their size and composition that are consistent with both the chemical information and with previously reported results from other methods of investigation.

Acknowledgements

The authors are thankful for financial support from the NRC-Helmholtz and the trilateral NRC Taiwan programs.

Appendix A. Diffraction by a collection of similar nano-particles of a perfect solid-solution alloy

We assume the alloy nano-particles to have same diameter, same composition and same basic structure. They only differ in the random way the atoms of the alloying element are distributed within a given nano-particle. We describe the electron density E_i in each individual nano-particle N_i as the sum of an average object A and a difference function D_i specific to the nano-particle. As the constituting atoms of the nano-particle are similar in radius and electron density, A is a positive function with large values, while D_i is a function with fairly small negative or positive values, which are randomly different from nano-particle to nano-particle. For a collection $i = 1,n$ of nano-particles in a sample of perfect solid-solution alloy, the distribution of D_i values has zero average.

The Fourier transform $F(E_i) = F(A + D_i)$ of the sum $A + D_i$ is the sum $F(A) + F(D_i)$. The diffracted intensity $I(E_i)$ is accordingly:

$$I(E_i) = (F(A) + F(D_i)) \times (F(A) + F(D_i))^* \quad (A.1)$$

where × is a multiplication and (*) denotes the complex conjugate. This is expanded as:

$$I(E_i) = F(A) \times F(A)^* + F(D_i) \times F(D_i)^* + F(A) \times F(D_i)^* + F(D_i) \times F(A)^* \quad (A.2)$$

The first two terms have real and positive values, and then add up in magnitudes. The sum of the last two terms is also real, but it can be positive, negative or zero just as well, depending on the particular atom distribution in nano-particle i. For a collection $i = 1,n$ of nano-particles, the sum of the last two terms then mostly cancels out. We can then write:

$$\sum_{i=1,n} (I(E_i)) \approx n \times F(A) \times F(A)^* + \sum_{i=1,n} (F(D_i) \times F(D_i)^*) \quad (A.3)$$

In other words, a collection of perfect solid-solution alloy nano-particles diffracts as if the average part and the random part of the electron distribution came from different objects and added in intensity, not in amplitude. Diffraction by an object with small and random positive or negative electron density is a small and random intensity contribution that is different from nano-particle to nano-particle.

Diffraction peaks from a collection of n nano-particles of a random solid-solution alloy are then n times those of the average nano-particle A sitting on a fairly constant intensity background that results from the superposition of the random intensity contribution of different nano-particles. This background gets eliminated in the numerical procedure detailed in the present paper. The above analysis made no use of the concept of periodicity and applies to nearly identical diffracting objects differing from one-another in a random way in their atom distribution. The above considerations then remain applicable, irrespective of whether the diffracted intensity calculation method is Debye's formula or a standard structure-factor calculation complemented by Scherrer's considerations for finite objects.

References

[1] W. Vielstich, A. Lamm, H.A. Gasteiger, Handbook of Fuel Cells: Fundamentals, Technology and Applications, vol. 2, John Wiley & Sons Inc., Chichester, 2005.
[2] J. McBreen, S. Mukerjee, in: A. Wieckowski (Ed.), Interfacial Electrochemistry, Marcel Dekker, New York, 1999, pp. 895–914.
[3] M.S. Nashner, A.I. Frenkel, D.L. Adler, J.R. Shapley, R.G. Nuzzo, J. Am. Chem. Soc. 119 (1997) 7760–7771.
[4] B.J. Hwang, C.-H. Chen, L.S. Sarma, J.M. Chen, G.-R. Wang, M.-T. Tang, D.-G. Liu, J.-F. Lee, J. Phys. Chem. B 110 (2006) 6475–6482.
[5] Y.Y. Tong, H.S. Kim, P.K. Babu, P. Waszczuk, A. Wieckowski, E. Oldfield, J. Am. Chem. Soc. 124 (2002) 468–473.
[6] C. Pan, F. Dassenoy, M.-J. Casanove, K. Philippot, C. Amiens, P. Lecante, A. Mosset, B. Chaudret, J. Phys. Chem. 103 (1999) 10098–10101.
[7] S. Park, A. Wieckowski, M.J. Weaver, J. Am. Chem. Soc. 125 (2003) 2282–2290.
[8] A. Lewera, W.P. Zhou, C. Vericat, J.H. Chung, R. Haasch, A. Wieckowski, P.S. Bagus, Electrochim. Acta 51 (2005) 3950–3956.
[9] W. Vogel, Cryst. Res. Technol. 33 (1998) 1141–1154.
[10] C. Roth, N. Martz, H. Fuess, Phys. Chem. Chem. Phys. 3 (2001) 315–319.
[11] L. Zhu, K.S. Liang, B. Zhang, J.S. Bradley, A.E. DePristo, J. Catal. 167 (1997) 412–416.
[12] C. Bock, C. Paquet, M. Couillard, G.A. Botton, B.R. MacDougall, J. Am. Chem. Soc. 126 (2004) 8028–8037.
[13] E.A. Baranova, C. Bock, D. Ilin, D. Wang, B. MacDougall, Surf. Sci. 600 (2006) 3502–3511.
[14] E.A. Baranova, C. Bock, D. Ilin, P.H.J. Mercier, X. Wu, D. Wang, B. MacDougall, in preparation.
[15] A.R. West, Solid State Chemistry and Its Applications, Wiley, New York, 1984.
[16] P. Debye, Ann. Phys. 46 (1915) 809.
[17] L. Vegard, Z. Phys. 5 (1921) 17–26.
[18] H.A. Gasteiger, P.N. Ross, E.J. Cairns, Surf. Sci. 293 (1993) 67–80.
[19] P.S. White, J.R. Rodgers, Y. Le Page, Acta Crystallogr. B58 (2002) 343–348.
[20] Y. Le Page, C. Bock, J.R. Rodgers, J. Alloys Compd. 422 (2006) 164–172.
[21] Y. Le Page, J.R. Rodgers, J. Appl. Crystallogr. 38 (2005) 697–705.
[22] International Tables for X-ray Crystallography, vol. IV, Kynoch Press, Birmingham, 1974.
[23] B.D. Cullity, Elements of X-ray Diffraction, Addison-Wesley Publishing Co., Inc., Reading, MA, 1956.
[24] C. Bock, B. MacDougall, Y. LePage, J. Electrochem. Soc. 151 (2004) A1269–A1278.
[25] J. Turkevich, G. Kim, Science 169 (1970) 873–879.
[26] N. Toshima, M. Harada, Y. Yamazaki, K. Asakura, J. Phys. Chem. 96 (1992) 9927–9933.
[27] M. Harada, K. Asakura, N. Toshima, J. Phys. Chem. 97 (1993) 5103–5113.
[28] T. Yonezawa, N. Toshima, J. Chem. Soc., Faraday Trans. 91 (1995) 4111–4115.
[29] N. Toshima, T. Yonezawa, New J. Chem. (1998) 1179–1201.